南京航空航天大学

论文集

（二〇〇一年）

第2册

一院

南京航空航天大学科技部编

二〇〇二年六月

一　院

○一三系

目 录

序号	姓 名	职 称	单位	论 文 题 目	刊物、会议名称	年、卷、期	类别
1	胡海岩 金栋平	正高 副高	013 013	Nonlinear dynamics of a suspended travelling cable subject to transverse fluid excitation	Journal of Sound and Vibration	0123903	H
2	胡海岩 郭大蕾 翁建生	正高 博士 博士	013 013 013	振动半主动控制技术的进展	振动、测试与诊断	012104	J
3	胡海岩	正高	013	线性受控系统的反馈时滞可辨识性	振动工程学报	011402	H
4	胡海岩	正高	013	Abundant dynamic features of a nonlinear system under delayed feedback control	Asia–Pacific Vibration Conference ' 2001	2001	
5	张文丰 胡海岩	博士 正高	013 013	含时滞的非线性动力系统参数辩识	振动工程学报	011403	H
6	张文丰 胡海岩	博士 正高	013 013	Modeling four-wheel-stearing vehicles for nonlinear dynamic simulation	Asia–Pacific Vibration Conference	2001	
7	韩 维 胡海岩 金栋平	博士 正高 副高	013 013 013	Vibro-impacts of a sleader cantilever beam with a lumped tip mass between two rigid stops	南京航空航天大学学报(英文版)	011802	J
8	钱小勇 胡海岩	硕士 正高	013 013	可调间隙的半主动吸振器及其实现	振动工程学报	011404	H
9	郭大蕾 胡海岩	博士 正高	013 013	具有可调增量的模糊–PID 电液主动控制悬架	振动工程学报	011403	H
10	王在华 胡海岩	博士 正高	013 013	Dinamics and reduction for nonlinear tine-delayed systems conposed of stlff and soft structures	Nonlinear Dynamics	012504	H
11	金栋平	副高	013	论高校力学类课程的创新教学	南京航空航天大学学报(社科版)	010314	
12	金栋平 胡海岩	副高 正高	013 013	随机碰撞振动的映射	新世纪力学研讨会-钱学森技术科学思想的回顾和展望(文集)	2001	
13	金栋平 胡海岩	副高 正高	013 013	Stretch and rotation of a suspended cabre subject to transrerse fruid excitation	Applied Mathematics and Mechanics	012208	H
14	金栋平 胡海岩	副高 正高	013 013	结构碰撞振动的建模与模态截断	固体力学学报	012202	H
15	金栋平 胡海岩	副高 正高	013 013	行进绳索在横向流体激励下的运动	力学学报	013304	H
16	金栋平 胡海岩	副高 正高	013 013	横向流激励下绳索的扩张和回转运动	应用数学和力学	012208	H
17	黄 睿 袁慎芳 陶宝祺	博士 正高 正高	013 013 013	含光纤编织复合材料试件的制作与实验研究	压电与声光	012302	J
18	黄 睿 袁慎芳	博士 正高	013 013	Intronsic microbend fiber optic sensors	International Symposium optoelectronic & Microelectronics 会议	2001	

序号	姓 名	职 称	单位	论 文 题 目	刊物、会议名称	年、卷、期	类别
19	黄 睿	博士	013	用于编织结构的光纤传感器的研究	材料导报	011506	H
	袁慎芳	正高	013				
	陶宝祺	正高	013				
20	杨 红	博士	013	空心光纤传感技术在断裂测量中的应用	传感技术学报	011401	J
	陶宝祺	正高	013				
	梁大开	正高	013				
21	杨 红	博士	013	光纤智能结构自诊断、自修复的研究	功能材料	013204	H
	梁大开	正高	013				
22	杨 红	博士	013	光纤应用于结构自修复的研究	材料保护	013401	H
	陶宝祺	正高	013				
	梁大开	正高	013				
23	沈文罡	硕士	013	The comparison of two typical consititution models of SMA	The first Asia-Pacific Workship on Smart Materials & Structure	2001	
	熊 克	副高	013				
24	袁慎芳	正高	013	应用小波分析及主动监测技术的复合材料损伤监测	材料工程	010002	H
	陶宝祺	正高	013				
	朱晓荣	博士	013				
25	熊 克	副高	013	Research on 1-3 orthogonal anisotropic piezoelectric composite material sensors	第三届世界结构健康监测会议	2001	
26	史治宇	正高	013	动力涡轮叶片的静动特性分析	工程力学学报	2001 增刊	
	王鑫伟	正高	013				
27	王鑫伟	正高	013	Recent developments in smart materials and structures in the aeronautical science key laboratory for smart materials & structures	The 3rd International Workshop on Structural Health Monitoring	2001	
	许希武	正高	013				
	熊 克	副高	013				
28	宁志威	博士	013	声-超声技术在碳-碳复合材料薄板损伤检测中的应用	振动、测试与诊断	012101	J
	孙良新	正高	013				
29	徐庆华	副高	013	踏板式摩托车振动试验研究	振动工程学报	0114 增刊	H
	周传荣	正高	013				
30	张雪华	副高	013	高强复合纤维在桥梁结构加固中的应用	东北公路	012404	
	史丽远	中级	013				
	艾 军	正高	013				
31	张雪华	副高	013	路桥衔接板块高性能耐冲磨砼的研究	森林工程	011705	
	姜正平	副高	013				
32	张雪华	副高	013	水泥砼路面快速修补技术的研究与应用	森林工程	011706	
	艾 军	正高	013				
	姜正平	副高	013				
33	周杰明	副高	013	多轴承动载下摆动疲劳试验方法	实验力学	011603	J
	汪 勇	副高	013				
	王庆德	副高	013				
34	沈海军	博士后	013	VB 中创建文本朗读应用程序	电脑学习	019706	
35	沈海军	博士后	013	具有“发送 E-mail”功能的 VB 应用程序	电脑学习	019705	
	田菩提	中级	机关				
36	沈海军	博士后	013	LC9 铝合金应力腐蚀特性试验研究	全国环境与断裂研讨会	2001	
	郭万林	正高	013				

Journal of Sound and Vibration (2001) **239**(3), 515–529
doi:10.1006/jsvi.2000.3161, available online at http://www.idealibrary.com on IDEAL®

NON-LINEAR DYNAMICS OF A SUSPENDED TRAVELLING CABLE SUBJECT TO TRANSVERSE FLUID EXCITATION

H. Y. Hu and D. P. Jin

Institute of Vibration Engineering Research, Nanjing University of Aeronautics and Astronautics, 210016 Nanjing, People's Republic of China. E-mail: hhyae@nuaa.edu.cn

(*Received* 23 *March* 2000, *and in final form* 20 *June* 2000)

Starting with the analysis of the fluid drag and lift on a suspended travelling cable subjected to transverse fluid excitation, the paper presents the expression of forces on the cable, and then a set of partial differential equations of in-plane and out-of-plane motions of the cable. In the case of small ratio of sag to span, the in-plane and out-of-plane modes of the first order dominate the motions of cable. Thus, the partial differential equations of cable are reduced to two ordinary differential equations of the second order by means of the Galerkin approach. Because the stiffness terms disappear in the ordinary differential equations when the cable is at equilibrium position, the co-ordinate transform proposed by Pilipchuk is used to describe the stretch and rotation of mid-span section of cable from the equilibrium position so that the transformed differential equations include linear stiffness terms. Afterwards, the differential equations are simplified by using the perturbation approach of two variables under the assumption that the Young's module of cable is not very small. As a result, the approximate cable dynamics yields a two-dimensional autonomous system and does not exhibit any chaotic motions. According to the approximated model, two equilibrium positions of cable are determined and their stability is analyzed. Finally, the influences of travelling velocity and cable density on the cable dynamics are discussed on the basis of numerical computations. The case studies show that the travelling velocity should be limited when a very light cable is laid under water in order to avoid harmful and dangerous swings.

1. INTRODUCTION

Suspended travelling cables are extensively used in various fields of engineering. The observed cable dynamics often exhibits complex non-linear behavior. Here are a few, but typical examples. (1) The cable of shipping crane may have aperiodic swings and produce poor position accuracy. (2) The balloon formation in ring spinning process often limits the moving speed of the yarn. (3) The tethered satellite deployed from an orbiting shuttle may undergo very complex vibration. Hence, it is essential to understand and predict the complicated non-linear dynamics of suspended travelling cables in their design phase.

In marine engineering, the dynamics of underwater cables, as an important topic, has drawn much attention since 1970s. For example, Choo and Casarella reviewed the early work on the mathematical models for anchoring cables with hydrodynamics taken into account [1]. Nair and Hung analyzed the stability of a towing cable immersed in water [2, 3]. Papazoglou and his co-authors made an experiment on the non-linear response of a cable immersed in water [4]. Recently, Vassalos and Huang summarized four types of analysis methods for the marine cable dynamics and presented the numerical simulation and experiment of a marine cable, one of ends of which is subjected to horizontal excitation

0022-460X/01/030515 + 15 $35.00/0

[5]. Mavrakos and Chatjigeorgiou studied the dynamic behavior of mooring cable with submerged buoys [6]. They found a way to reduce the dynamic tension of the cable by properly choosing buoys and their positions. Chang and his co-authors presented a detailed analysis of non-linear interaction of the first two in-plane modes of a suspended cable subjected to a fluid flow in direction of cable [7]. To the authors' knowledge, however, the non-linear dynamics of suspended travelling cables subject to transverse fluid flow is still an open problem.

When an underwater cable is being laid, it is travelling at certain velocity. This makes the cable dynamics are complicated than a suspended cable. Intensive studies have been made for the dynamics of travelling cable in air, such as the deployed cable of a tethered satellite, tapes of video recorder. For example, Pekins and Mote Jr. established the three-dimensional non-linear dynamic model for an arbitrarily sagged travelling cable with arbitrarily inclined eyelets in air by using the description of finite strain [8]. Compared with those studies, the dynamics of underwater cable is a tougher problem.

The aim of this paper is to reveal the dynamics of a suspended travelling cable under the transverse fluid flow. The paper is organized as follows. To properly describe the cable dynamics, the fluid drag and the lift on the cable are analyzed first. Then a set of partial differential equations of motion is established. The Galerkin approach, the Pilipchuk transform and the perturbation technique of two variables are successively used to simplify the partial differential equations to a two-dimensional autonomous system. Afterwards, the equilibrium positions and their stability are analyzed in detail. Finally, some case studies are discussed.

2. MODEL OF A SUSPENDED TRAVELLING CABLE

As shown in Figure 1, a cable, subjected to a transverse, uniformly distributed fluid flow at constant velocity V_f, is moving at constant velocity c through two eyelets spanned under water. The dashed curve in Figure 1 represents the static configuration of cable in still water. To describe the motion of cable, a set of Cartesian co-ordinates is established in Figure 1 such that the x-axis connects the two eyelets, the y-axis is on the horizontal plane and perpendicular to x-axis, and the z-axis points the direction of gravity. In addition, an arc co-ordinate s is introduced along the cable to position the specific section of the cable.

In the frame of Cartesian co-ordinates, the fluid flow moves in the y direction and drives an arbitrary inertial point of the travelling cable from the spatial position $P^i(x, v_0, w_0)$ to $P^f(x + u, v, w)$ as shown in Figure 1. The accurate modelling of a cable gives rise to a non-linear dynamic system having infinite degrees of freedom. In the case of small ratio of

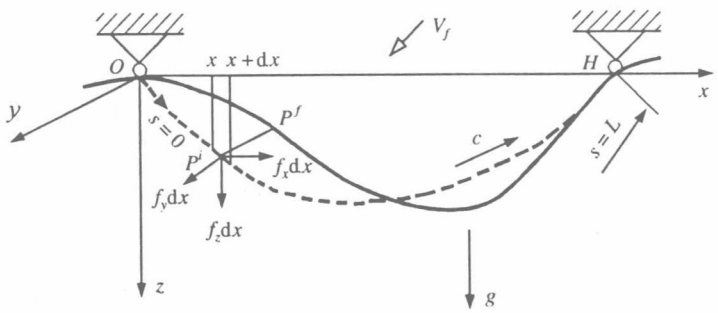

Figure 1. A suspended travelling cable subjected to transverse fluid flow.

where

$$b = \sqrt{1 + \lambda_0^2}, \quad \bar{k} = \frac{\lambda_0}{1 + \lambda_0^2}, \quad \lambda_0 = \frac{c}{V_f}. \tag{4}$$

By substituting the following geometric relations:

$$\cos\beta = \frac{(1 - \lambda_0 v')V_f}{V_r}, \quad \cos\beta_3 = \frac{V_f - \dot{v}}{V_f}, \quad \sin\beta_3 = \frac{\dot{w}}{V_f}, \quad \cos\beta_4 \approx 1 \tag{5}$$

into equation (2), one obtains the components of fluid force on the cable element of unit length

$$\begin{aligned} f_y &= -\tfrac{1}{2}\rho_f b D_C V_f[bC_L\dot{w}(1 - \bar{k}v') - C_D(V_f - \dot{v})(1 - \lambda_0 v')](1 - \bar{k}v'), \\ f_z &= -\tfrac{1}{2}\rho_f b D_C V_f[bC_L(V_f - \dot{v})(1 - \bar{k}v') + C_D\dot{w}(1 - \lambda_0 v')](1 - \bar{k}v'). \end{aligned} \tag{6}$$

According to the Hamilton principle, one can derive a set of partial equations that govern the dynamics of suspended travelling cable as follows:

$$\frac{\partial^2 v}{\partial t^2} - \frac{\partial^2 v}{\partial s^2}\frac{E}{\rho}\bar{\varepsilon} = \frac{f_y}{\rho A}, \qquad \frac{\partial^2 w}{\partial t^2} - \frac{\partial^2 w}{\partial s^2}\frac{E}{\rho}\bar{\varepsilon} = \frac{f_z}{\rho A} + \bar{g}, \tag{7}$$

where

$$\rho = \rho_c + C_I\rho_f, \quad \bar{g} = \frac{g\rho_c}{\rho}, \tag{8}$$

ρ_c is the density of the cable, C_I the coefficient of fluid inertial attached to the cable, g the gravitational acceleration, A the section area of cable, E the Young's module of cable, and $\bar{\varepsilon}$ the averaged longitudinal stain of cable as defined in reference [7]:

$$\bar{\varepsilon}(t) = \frac{1}{2H}\int_0^H \left[\left(\frac{\partial v}{\partial x}\right)^2 + \left(\frac{\partial w}{\partial x}\right)^2 - \left(\frac{\partial w_0}{\partial x}\right)^2\right] \mathrm{d}x. \tag{9}$$

Here $w_0(x) = D\sin(\pi x/H)$ is the static configuration of the cable at the equilibrium position in still water, H the span of cable, and D the sag of cable in the absence of gravity.

3. SYSTEM REDUCTION AND PILIPCHUK TRANSFORM

To simplify the dynamic equation (7) with the expressions of fluid force substituted, a set of new variables and parameters are defined first

$$\begin{aligned} &\eta = \frac{x}{H}, \quad V = \frac{v}{D}, \quad W = \frac{w}{D}, \quad \tau = \frac{d}{H}\sqrt{\frac{E}{\rho}}t, \quad d = \frac{D}{H}, \quad \mu = \sqrt{\frac{\rho_c g H^4}{ED^3}}, \\ &c_f = \frac{C_L}{C_D}, \quad v_f = \frac{V_f}{d^2}\sqrt{\frac{\rho}{E}}, \quad D_f = \frac{b\rho_f v_f C_D D_C D}{2\rho A}, \quad \lambda = d\lambda_0, \quad k = d\bar{k}. \end{aligned} \tag{10}$$

Then, the in-plane and out-of-plane motions of cable are approximated by the vibration modes of the first order as follows:

$$V(\eta, \tau) = \sin(\pi\eta)q_1(\tau), \qquad W(\eta, \tau) = \sin(\pi\eta)q_2(\tau). \tag{11}$$

By means of the Galerkin approach, equation (7), with equation (6) substituted, is simplified as

$$\begin{aligned}\ddot{q}_1 + \varepsilon_q q_1 &= -D_f\{m\dot{q}_2 + \dot{q}_1 - \delta_1 v_f + \sigma q_1^2[m\dot{q}_2 + n(\dot{q}_1 - \delta_2 v_f)]\},\\ \ddot{q}_2 + \varepsilon_q q_2 &= -D_f\{\dot{q}_2 - m(\dot{q}_1 - \delta_1 v_f) + \sigma q_1^2[n\dot{q}_2 - m(\dot{q}_1 - \delta_2 v_f)]\} + \delta_1 \mu^2,\end{aligned} \tag{12}$$

where

$$\varepsilon_q = \frac{\bar{\varepsilon}}{d^2} = \frac{\pi^2}{4}(q_1^2 + q_2^2 - 1), \quad \sigma = \frac{k^2\pi^2}{4}, \quad m = bc_f, \quad n = 1 + \lambda_0^2, \quad \delta_1 = \frac{4}{\pi}, \quad \delta_2 = \frac{16}{3\pi}. \tag{13}$$

The dot in equation (12) is redefined as the derivative with respect to the dimensionless time τ. This equation governs the horizontal and vertical motions of the mid-span section of cable.

Intuitively speaking, the motion of mid-span section of cable is similar to that of a spring pendulum of two degrees of freedom. Like the study on the spring pendulum, it is very natural to consider a co-ordinate transform suggested by Pilipchuk in reference [9]:

$$q_1(\tau) = [1 + \xi(\tau)] \sin \varphi(\tau), \qquad q_2(\tau) = [1 + \xi(\tau)] \cos \varphi(\tau), \tag{14}$$

where $\xi(\tau)$ and $\varphi(\tau)$ are the radial stretch and the rotation angle of mid-span section of cable respectively. As shown in Figure 3, φ is measured from the bottom position of cable, where the cable is at rest in still water, and in clockwise direction.

From equation (14), one can see that $\xi = 0$ corresponds to the circular motion of mid-span section of cable. For this kind of motion, one has

$$\varepsilon_q = \frac{\pi^2}{4}(q_1^2 + q_2^2 - 1) = 0. \tag{15}$$

Equation (15) indicates that the averaged longitudinal strain of cable vanishes when the mid-span section of cable moves exactly on the unit circle. So do all the stiffness terms in equation (12). This phenomenon usually makes a trouble to the perturbation analysis. One can immediately find, however, that in the new co-ordinates, at least one dynamic equation remains a stiffness term.

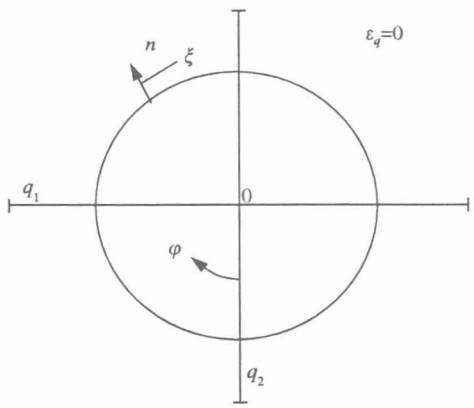

Figure 3. Definition of new variables in Pilipchuk transform.

By substituting transform (14) into Equation (12) and neglecting the higher order terms of ξ, one obtains a set of dynamic equations that govern the stretch and rotation of mid-span section of cable as following:

$$\ddot{\xi} + D_f\dot{\xi} + \omega_0^2\xi - (mD_f - \dot{\varphi})\dot{\varphi} - \frac{dF(\varphi)}{d\varphi} + G(\dot{\xi}, \varphi, \dot{\varphi})\sin^2\varphi = 0, \tag{16a}$$

$$\ddot{\varphi} + D_f\dot{\varphi} + (mD_f + 2\dot{\varphi})\dot{\xi} + F(\varphi) + H(\dot{\xi}, \varphi, \dot{\varphi})\sin^2\varphi = 0, \tag{16b}$$

where

$$\begin{aligned} F(\varphi) &= \delta_1[(\mu^2 - mD_f v_f)\sin\varphi - D_f v_f\cos\varphi], \\ G(\dot{\xi}, \varphi, \dot{\varphi}) &= \sigma_1(n\dot{\xi} - m\dot{\varphi}) - 4\sigma_2(n\sin\varphi - m\cos\varphi), \\ H(\dot{\xi}, \varphi, \dot{\varphi}) &= \sigma_1(m\dot{\xi} + n\dot{\varphi}) - 4\sigma_2(m\sin\varphi + n\cos\varphi) \end{aligned} \tag{17}$$

and

$$\omega_0 = \frac{\pi^2}{\sqrt{2}}, \quad \sigma_1 = \frac{\pi^2 k^2 D_f}{4}, \quad \sigma_2 = \frac{\pi k^2 D_f v_f}{3}. \tag{18}$$

Now, the elastic restoring force in cable gives rise to the static stiffness terms in equation (16a) as long as the motion of mid-span section of cable deviates from the unit circle. Even if the mid-span section of cable is moving along the unit circle, the effects of gravity, fluid drag and lift still offer a stiffness term to equation (16b).

4. APPROXIMATE SOLUTION

To further simplify equation (16), an important phenomenon of cable dynamics should be noticed. That is, the magnitude of radial stretch of mid-span section of cable is usually much smaller than the magnitude of rotation angle since the Young's module of a real cable cannot be very small. This is the case when the cable is made of metal or even glass fibre. In most cases, the assumption of $E \gg \rho_c g H^4/D^3$ holds true, there follows a small parameter μ according to its definition in equation (10). When a steel cable under water is taken as an example, the curves of small μ versus H for some practical ratios of sag-to-span are shown in Figure 4.

In the case of small μ, the perturbation technique can be used to give an approximate analysis of cable dynamics under the transverse fluid flow. For this purpose, one can rescale the time, generalized displacements and two parameters as follows:

$$t_0 = \mu\tau, \quad \xi = \mu^2\bar{\xi}(\tau), \quad \varphi = \hat{\varphi}(\mu\tau) + \mu^2\bar{\varphi}(\tau), \quad D_f = \mu\bar{D}_f, \quad v_f = \mu\bar{v}_f. \tag{19}$$

By substituting equation (19) into equation (16) and dropping the higher order terms, one obtains

$$\begin{aligned} \ddot{\bar{\xi}} + \omega_0^2\bar{\xi} &= -\left(\frac{d\hat{\varphi}}{dt_0}\right)^2 + 2\mu\dot{\bar{\varphi}}\frac{d\hat{\varphi}}{dt_0} + \bar{Q}_1\left(\frac{d\hat{\varphi}}{dt_0} + \mu\dot{\bar{\varphi}}\right) - \bar{Q}_2\mu\dot{\bar{\xi}} + \bar{Q}_3\sin\hat{\varphi} + \bar{Q}_4\cos\hat{\varphi}, \\ \ddot{\bar{\varphi}} &= -\frac{d^2\hat{\varphi}}{dt_0^2} - 2\mu\dot{\bar{\xi}}\frac{d\hat{\varphi}}{dt_0} - \bar{Q}_2\left(\frac{d\hat{\varphi}}{dt_0} + \mu\dot{\bar{\varphi}}\right) - \bar{Q}_1\mu\dot{\bar{\xi}} - \bar{Q}_4\sin\hat{\varphi} + \bar{Q}_3\cos\hat{\varphi}, \end{aligned} \tag{20}$$

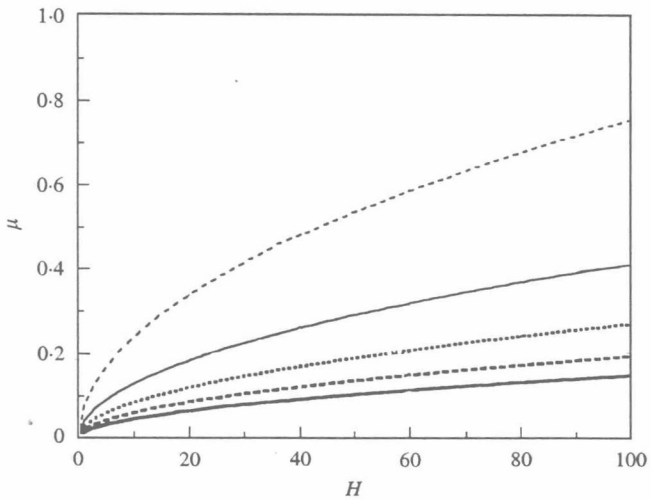

Figure 4. Small parameter μ versus span H at practical ratios of sag-to-span ($g = 9{\cdot}8$ m/s^2, $\rho_c = 7{\cdot}8 \times 10^3$ kg/m^3, $E = 210$ GPa). ——, $d = 0{\cdot}12$; - - - -, $d = 0{\cdot}10$; ·····, $d = 0{\cdot}08$; ——, $d = 0{\cdot}06$; - - - - -, $d = 0{\cdot}04$.

where

$$\bar{\sigma}_1 = \frac{k^2\pi^2\bar{D}_f}{4}, \quad \bar{\sigma}_2 = \frac{k^2\pi\bar{D}_f\bar{v}_f}{3},$$

$$\bar{Q}_1 = m(\bar{D}_f + \bar{\sigma}_1 \sin^2\hat{\varphi}), \quad \bar{Q}_2 = \bar{D}_f + n\bar{\sigma}_1 \sin^2\hat{\varphi}, \tag{21}$$

$$\bar{Q}_3 = \delta_1(\bar{D}_f\bar{v}_f + \pi n\bar{\sigma}_2 \sin^2\hat{\varphi}), \quad \bar{Q}_4 = \delta_1[1 - m(\bar{D}_f\bar{v}_f + \pi\bar{\sigma}_2 \sin^2\hat{\varphi})].$$

Let $\tilde{t} = \omega_0\tau$ be a new dimensionless time scale, i.e., $\bar{\xi} = \bar{\xi}(\tilde{t}, t_0)$ and $\bar{\varphi} = \bar{\varphi}(\tilde{t}, t_0)$. It is easy to see that equation (20) involves a slow time scale t_0 and a fast time scale $\tilde{t}$. According to the two variable perturbation approach [10], the solution of equation (20) should be in the form

$$\begin{aligned} \bar{\xi} &= \bar{\xi}_0(\tilde{t}, t_0) + \mu\bar{\xi}_1(\tilde{t}, t_0) + O(\mu^2), \\ \bar{\varphi} &= \bar{\varphi}_0(\tilde{t}, t_0) + \mu\bar{\varphi}_1(\tilde{t}, t_0) + O(\mu^2). \end{aligned} \tag{22}$$

By substituting equation (22) into equation (20) and equating the same power of μ, one has

$$\omega_0^2\left(\frac{\partial^2\bar{\xi}_0}{\partial\tilde{t}^2} + \bar{\xi}_0\right) = -\left(\frac{\mathrm{d}\hat{\varphi}}{\mathrm{d}t_0}\right)^2 + \bar{Q}_1\frac{\mathrm{d}\hat{\varphi}}{\mathrm{d}t_0} + \bar{Q}_3 \sin\hat{\varphi} + \bar{Q}_4 \cos\hat{\varphi}, \tag{23}$$

$$\omega_0^2\frac{\partial^2\bar{\varphi}_0}{\partial\tilde{t}^2} = -\frac{\mathrm{d}^2\hat{\varphi}}{\mathrm{d}t_0^2} - \bar{Q}_2\frac{\mathrm{d}\hat{\varphi}}{\mathrm{d}t_0} - \bar{Q}_4 \sin\hat{\varphi} + \bar{Q}_3 \cos\hat{\varphi}, \tag{24}$$

$$\omega_0^2\left(\frac{\partial^2\bar{\xi}_1}{\partial\tilde{t}^2} + \bar{\xi}_1\right) = 2\omega_0\left(\frac{\mathrm{d}\hat{\varphi}}{\mathrm{d}t_0}\frac{\partial\bar{\varphi}_0}{\partial\tilde{t}} - \frac{\partial^2\bar{\xi}_0}{\partial\tilde{t}\partial t_0}\right) + \omega_0\left(\bar{Q}_1\frac{\partial\bar{\varphi}_0}{\partial\tilde{t}} - \bar{Q}_2\frac{\partial\bar{\xi}_0}{\partial\tilde{t}}\right), \tag{25}$$

$$\omega_0^2\frac{\partial^2\bar{\varphi}_1}{\partial\tilde{t}^2} = -2\omega_0\frac{\mathrm{d}\hat{\varphi}}{\mathrm{d}t_0}\frac{\partial\bar{\xi}_0}{\partial\tilde{t}} - \omega_0\left(\bar{Q}_2\frac{\partial\bar{\varphi}_0}{\partial\tilde{t}} + \bar{Q}_1\frac{\partial\bar{\xi}_0}{\partial\tilde{t}}\right). \tag{26}$$

Because the right-hand side of equation (23) involves the slow time scale t_0 only, the solution of equation (23) reads

$$\bar{\xi}_0 = A_0(t_0)\sin(\tilde{t}) + B_0(t_0)\cos(\tilde{t}) + \frac{1}{\omega_0^2}\left[-\left(\frac{\mathrm{d}\hat{\varphi}}{\mathrm{d}t_0}\right)^2 + \bar{Q}_1\frac{\mathrm{d}\hat{\varphi}}{\mathrm{d}t_0} + \bar{Q}_3\sin\hat{\varphi} + \bar{Q}_4\cos\hat{\varphi}\right], \quad (27)$$

where $A_0(t_0)$ and $B_0(t_0)$ are the functions in slow time scale. Similarly, solving equation (24) for $\bar{\varphi}_0$ and dropping the secular terms give

$$\bar{\varphi}_0 = 0. \quad (28)$$

From the cancellation condition of secular terms in equations (25) and (26), one can find the approximate solution of the first order for equation (16):

$$\xi = \mu^2(\alpha_0\sin\omega_0\tau + \beta_0\cos\omega_0\tau)\mathrm{e}^{-Q_2\tau} + \frac{1}{\omega_0^2}\left[-\left(\frac{\mathrm{d}\hat{\varphi}}{\mathrm{d}\tau}\right)^2 + Q_1\frac{\mathrm{d}\hat{\varphi}}{\mathrm{d}\tau} + Q_3\sin\hat{\varphi} + Q_4\cos\hat{\varphi}\right], \quad (29)$$

$$\varphi = \hat{\varphi} + \frac{\mu^2}{\omega_0}\left(2\frac{\mathrm{d}\hat{\varphi}}{\mathrm{d}\tau} + Q_1\right)(\alpha_0\cos\omega_0\tau - \beta_0\sin\omega_0\tau)\mathrm{e}^{-Q_2\tau},$$

where α_0 and β_0 are the arbitrary parameters determined by the initial conditions, whereas

$$Q_1 = mD_f + \sigma_1\sin^2\hat{\varphi}, \qquad Q_2 = D_f + n\sigma_1\sin^2\hat{\varphi},$$
$$Q_3 = \delta_1(D_f v_f + \pi n\sigma_2\sin^2\hat{\varphi}), \qquad Q_4 = \delta_1[\mu^2 - m(D_f v_f + \pi\sigma_2\sin^2\hat{\varphi})]. \quad (30)$$

From equations (24) and (28), one can see that $\hat{\varphi}$ yields

$$\frac{\mathrm{d}^2\hat{\varphi}}{\mathrm{d}\tau^2} + Q_2\frac{\mathrm{d}\hat{\varphi}}{\mathrm{d}\tau} + Q_4\sin\hat{\varphi} - Q_3\cos\hat{\varphi} = 0. \quad (31)$$

In the sense of the first order approximation, equation (31) serves as a simplified dynamic equation of the original cable system. As equation (31) is equivalent to a two-dimensional autonomous system, the approximated model of cable does not exhibit any chaotic motions. Furthermore, Q_2, the coefficient of velocity term, involves the parameter $D_f > 0$ and keeps positive. Hence, the system is energy dissipative and does not undergo any Hopf bifurcation.

5. STABILITY ANALYSIS OF EQUILIBRIUM POSITIONS

5.1. DETERMINATION OF EQUILIBRIUM POSITIONS

From equation (16), the equilibrium position (φ_0, ξ_0) yields

$$\omega_0^2\xi_0 - \frac{\mathrm{d}F(\varphi_0)}{\mathrm{d}\varphi_0} + G(0, \varphi_0, 0)\sin^2\varphi_0 = 0, \qquad F(\varphi_0) + H(0, \varphi_0, 0)\sin^2\varphi_0 = 0, \quad (32a,b)$$

namely

$$\xi_0 = \frac{1}{\omega_0^2}\left[\frac{\mathrm{d}F(\varphi_0)}{\mathrm{d}\varphi_0} + 4\sigma_2(n\sin\varphi_0 - m\cos\varphi_0)\sin^2\varphi_0\right], \quad (33a)$$

$$F(\varphi_0) - 4\sigma_2(m\sin\varphi_0 + n\cos\varphi_0)\sin^2\varphi_0 = 0. \quad (33b)$$

One can first solve equation (33b) for the rotation angle φ_0 and then gets the radial stretch ξ_0 from equation (33a).

For simplicity, first consider the case when the cable is not travelling in direction x, i.e., $c = 0$. This results in

$$\lambda_0 = 0, \quad m = c_f, \quad n = 1, \quad \sigma_2 = 0 \tag{34}$$

such that equation (33) is simplified as

$$\xi_0 = \frac{1}{\omega_0^2}\frac{\mathrm{d}F(\varphi_0)}{\mathrm{d}\varphi_0} = \frac{8}{\pi^5}[(\mu^2 - c_f v_f D_f)\cos\varphi_0 + v_f D_f \sin\varphi_0] \tag{35a}$$

$$F(\varphi_0) = \delta_1[(\mu^2 - c_f v_f D_f)\sin\varphi_0 - v_f D_f \cos\varphi_0] = 0. \tag{35b}$$

Solving equation (35b) for φ_0 gives two possible angles of equilibrium

$$\varphi_{01} = \arccos\frac{\mu^2 - c_f v_f D_f}{\sqrt{(\mu^2 - c_f v_f D_f)^2 + (v_f D_f)^2}} \in (0, \pi), \quad \varphi_{02} = \varphi_{01} + \pi \in (\pi, 2\pi). \tag{36}$$

The corresponding values of radial stretch are

$$\xi_{01,2} = \pm\frac{8}{\pi^5}\sqrt{(\mu^2 - c_f v_f D_f)^2 + (v_f D_f)^2}. \tag{37}$$

According to Figure 3, the equilibrium positions corresponding to (φ_{01}, ξ_{01}) and (φ_{02}, ξ_{02}) are referred to as the left equilibrium position and the right equilibrium position respectively.

In the case of $\mu^2 > c_f v_f D_f$, one has $\varphi_{01} \in (0, \pi/2)$ and $\varphi_{02} \in (\pi, 3\pi/2)$. That is, the left equilibrium position is below the x-axis and the right one is above the x-axis. If $\mu^2 < c_f v_f D_f$, the reverse order can be observed. An interesting phenomenon is the critical case when two equilibrium positions happen to be on the horizontal plane, i.e., $\varphi_{01} = \pi/2$ and $\varphi_{02} = -\pi/2$, if $\mu^2 = c_f v_f D_f$. Substituting the original system parameters into this equation, one arrives at

$$\rho_c A g = \tfrac{1}{2}\rho_f D_C C_L V_r^2 \equiv |F_L|. \tag{38}$$

This indicates that the weight of cable of unit length is just balanced by the lift of fluid flow on the cable segment. As a consequent result, the tension in cable is balanced by the fluid drag only. In this case, the radial stretch of cable reached its minimum $8v_f D_f/\pi^5$. Obviously, this case happens only when $c_f > 0$ and $v_f > 0$ since D_f is proportional to v_f, and $\mu > 0$. Hence, the conditions of $C_L > 0$ and $V_f > 0$ should hold true. That is, the cable must be subjected to the transverse fluid flow that produces enough fluid lift.

When the cable is travelling in x direction, a more detailed form of equation (33b) reads

$$[\mu^2 - m(v_f D_f + \pi\sigma_2 \sin^2\varphi_0)]\sin\varphi_0 - (D_f v_f + n\pi\sigma_2 \sin^2\varphi_0)\cos\varphi_0 = 0. \tag{39}$$

By means of $\theta = \sin^2\varphi_0$, equation (39) can be tansformed to

$$a_0\theta^3 + a_1\theta^2 + a_2\theta + a_3 = 0, \tag{40}$$

where

$$a_0 = \pi^2\sigma_2^2(m^2 + n^2) \geqslant 0, \quad a_1 = \pi\sigma_2[2v_f D_f(m^2 + n) - (2m\mu^2 + \pi\sigma_2 n^2)],$$
$$a_2 = (\mu^2 - mv_f D_f)^2 + v_f^2 D_f^2 - 2\pi n\sigma_2 v_f D_f, \qquad a_3 = -v_f^2 D_f^2 < 0. \tag{41}$$

It can be proved, through a lengthy algebraic manipulation on MAPLE, that equation (40) has only one positive real root $\theta_1 \in [0, 1]$, which corresponds to two actual roots and two pseudo-roots of equation (39). With the help of equation (39), the two pseudo-roots can be removed and a pair of rotation angles of equilibrium position is determined as follows:

$$\varphi_{01} = \arccos \frac{\mu^2 - m(v_f D_f + \pi\sigma_2\theta_1)}{\sqrt{[\mu^2 - m(v_f D_f + \pi\sigma_2\theta_1)]^2 + (D_f v_f + n\pi\sigma_2\theta_1)^2}} \in (0, \pi),$$
$$\varphi_{02} = \varphi_{01} + \pi \in (\pi, 2\pi). \tag{42}$$

Then, equation (33a) gives the corresponding solutions of radial stretch.

5.2. STABILITY ANALYSIS

In order to analyze the stability of equilibrium positions, one should study the linear perturbation in equation (16) at (φ_{0i}, ξ_{0i}), i = 1, 2. To simplify this procedure, recall the approximate solution (ξ, φ) given by equation (29) near the equilibrium position. Because $Q_2 > 0$, (ξ, φ) possesses the same stability property as $\hat{\varphi}$ governed by equation (31). Consider the perturbed equation of equation (31) at a rotation angle φ_{0i} of equilibrium position

$$\frac{d^2\Delta\hat{\varphi}}{d\tau^2} + D_f\frac{d\Delta\hat{\varphi}}{d\tau} + \left[\left(Q_3 + \frac{\partial Q_4}{\partial\varphi_{0i}}\right)\sin\varphi_{0i} + \left(Q_4 - \frac{\partial Q_3}{\partial\varphi_{0i}}\right)\cos\varphi_{0i}\right]\Delta\hat{\varphi} = 0. \tag{43}$$

As $D_f > 0$, equation (43) is asymptotically stable if and only the following inequality holds true:

$$\left(Q_3 + \frac{\partial Q_4}{\partial\varphi_{0i}}\right)\sin\varphi_{0i} + \left(Q_4 - \frac{\partial Q_3}{\partial\varphi_{0i}}\right)\cos\varphi_{0i} > 0. \tag{44}$$

When the cable is not travelling, equation (44) can be simplified as

$$\frac{dF(\varphi_{0i})}{d\tau} = \delta_1[(\mu^2 - c_f v_f D_f)\cos\varphi_{0i} + v_f D_f \sin\varphi_{0i}] > 0. \tag{45}$$

Substituting equation (36) into equation (45) gives

$$\frac{dF(\varphi_{01})}{d\tau} = \frac{\delta_1}{\sqrt{(\mu^2 - c_f v_f D_f)^2 + (v_f D_f)^2}} > 0, \tag{46a}$$

$$\frac{dF(\varphi_{02})}{d\tau} = \frac{\delta_1}{\sqrt{(\mu^2 - c_f v_f D_f)^2 + (v_f D_f)^2}} < 0. \tag{46b}$$

Hence, the left equilibrium position is always asymptotically stable and the right equilibrium position is unstable when the fluid flows from the right to the left. It is easy to see that the right equilibrium position is a saddle point.

In the case of travelling cable, it seems impossible to derive an analytical stability criterion like equation (46) for the equilibrium positions. However, the tuition and a great number of numerical examples support the similar assertion. That is, the left equilibrium position is asymptotically stable.

6. CASE STUDIES

6.1. ACCURACY OF APPROXIMATE SOLUTION

To check the accuracy of approximate solution (29) determined by equation (31) with a small parameter μ, a great number of numerical comparisons were made between the

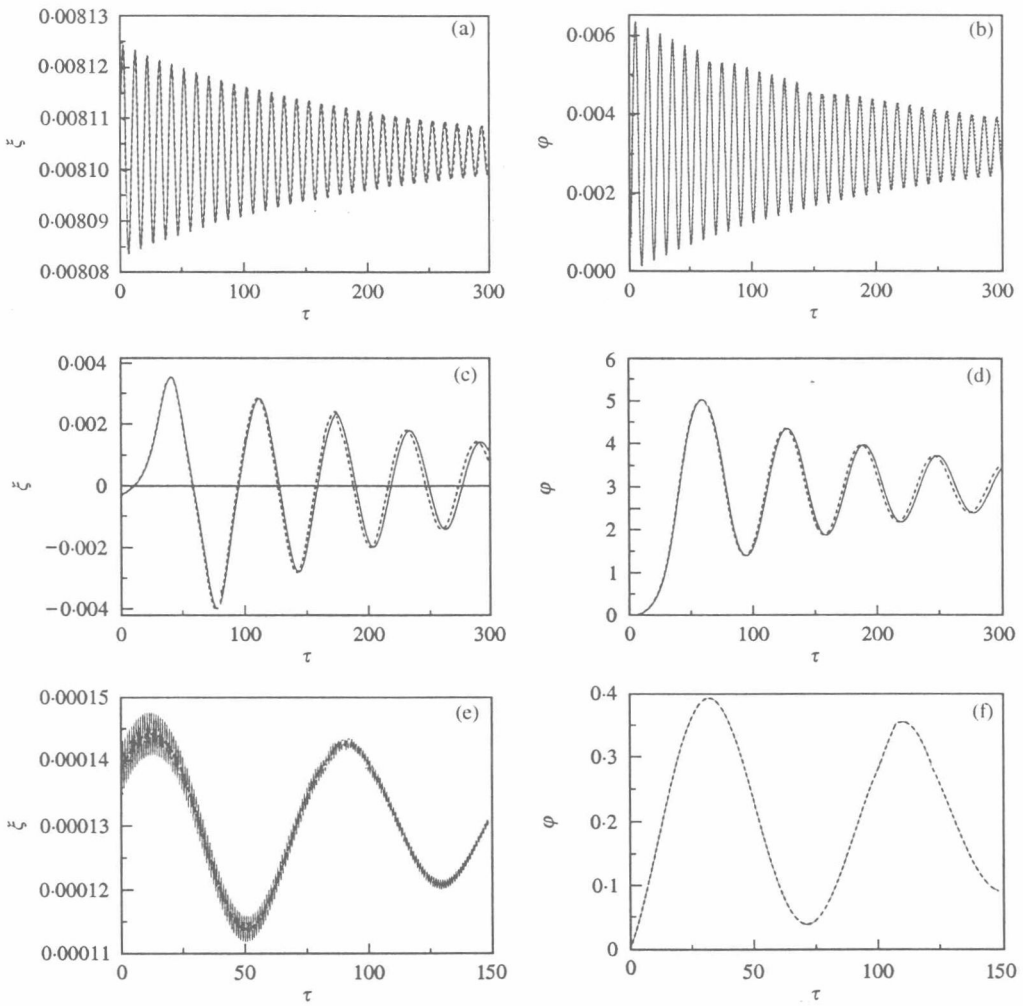

Figure 5. Comparison between solutions of equations (16) and (31) ($d = 0{\cdot}1$, $c_f = 0{\cdot}5$, $v_f = 0{\cdot}1$, $D_f = 0{\cdot}1$). (a) Stretch ($\mu = 0{\cdot}6$, $\lambda_0 = 100$); (b) Rotation angle ($\mu = 0{\cdot}6$, $\lambda_0 = 100$); (c) Stretch ($\mu = 0{\cdot}3$, $\lambda_0 = 200$); (d) Rotation angle ($\mu = 0{\cdot}3$, $\lambda_0 = 200$); (e) Stretch ($\mu = 0{\cdot}1$, $\lambda_0 = 10$); (f) Rotation angle ($\mu = 0{\cdot}1$, $\lambda_0 = 10$), ——, exact; - - - - -, approximate.

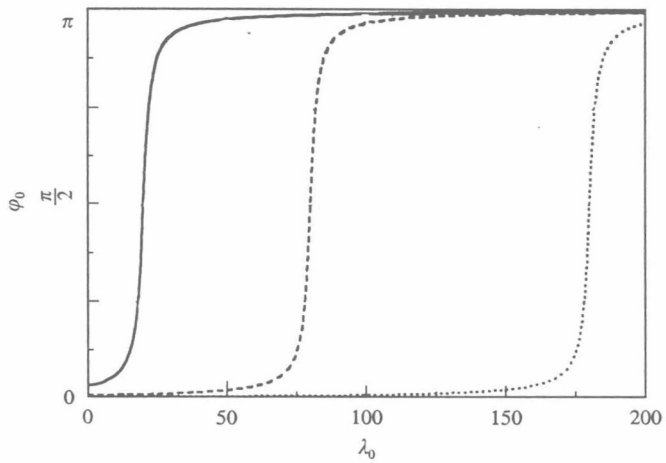

Figure 6. Rotation angle of stable equilibrium position versus relative travelling velocity for three specific values of μ ($d = 0{\cdot}1$, $c_f = 0{\cdot}5$, $v_f = 0{\cdot}1$, $D_f = 0{\cdot}1$). ——, $\mu = 0{\cdot}1$; - - - - -, $\mu = 0{\cdot}2$; ·····, $\mu = 0{\cdot}3$.

approximate solution and the numerical solution of equation (16), which is referred to as "exact solution" for short. All the numerical examples showed very good agreement between those two kinds of solutions in a wide range of parameters. For example, it is very hard to identify the difference between the exact and approximate solution shown in Figures 5(a) and 5(b) even for $\mu = 0{\cdot}6$ and $\lambda_0 = 100$. Figures 5(c) and 5(d) show an identifiable, but very small difference between the exact and approximate solutions when the travelling velocity was so high that $\lim_{\tau \to +\infty} \varphi(\tau) \to 3{\cdot}04$, i.e., the mid-span section of cable arrived at the top equilibrium position.

It should be pointed out that in the above two case studies, the initial state of solution (29) was set to meet the requirement of $\varphi_0(0) = 0$, $\dot{\varphi}_0(0) = 0$, $\alpha_0 = 0$, $\beta_0 = 0$, and so was the state of exact solution. As a result, the high-frequency components do not appear in the stretch and rotation of cable. To show the accuracy of approximate solution when the exact solution involves high-frequency components, Figures 5(e) and (5(f) give the comparison of exact and approximate solutions when $\varphi_0(0) = 0$, $\dot{\varphi}_0(0) = 0{\cdot}01$, $\alpha_0 = 0$, $\beta_0 = 0$. In this case, the approximate stretch offers a kind of averaged slow trend, as shown in Figure 5(e), of the exact stretch, which engineers are interested in. As for the rotation angle, the approximate solution still coincides with the exact one as shown in Figure 5(f).

6.2. EFFECTS OF TRAVELLING VELOCITY AND CABLE DENSITY ON DYNAMICS

In this study, the system parameters were set at $d = 0{\cdot}1$, $c_f = 0{\cdot}5$, $D_f = 0{\cdot}1$, $v_f = 0{\cdot}1$, while parameters μ and λ_0 were taken as the two changeable parameters. As v_f was fixed, the change of λ_0 represents only the variation of travelling velocity c. In addition, the change of μ can be understood as the variation in cable density of ρ_c only, because D_f and v_f appear in the form of product in equation (31) so that the total density of cable system ρ disappears.

To gain an insight into the cable dynamics, the rotation angles of equilibrium position of cable were computed according to equations (40) and (42) first. Figure 6 shows the rotation angle of asymptotically stable equilibrium position of cable with increase of travelling velocity for three specific values of μ. The three curves in the similar shapes indicate that the stable equilibrium position always goes up from the bottom to the top with increase of

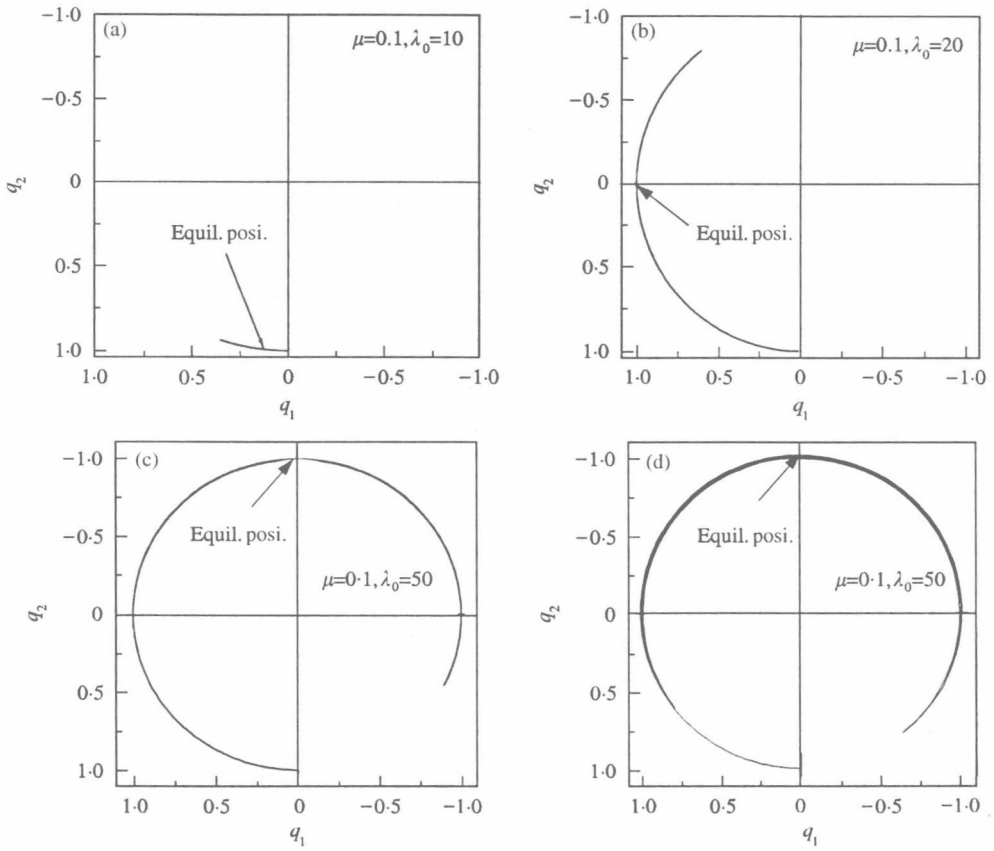

Figure 7. Motions of mid-span section of cable at different travelling velocities ($\mu = 0{\cdot}1$, $d = 0{\cdot}1$, $c_f = 0{\cdot}5$, $v_f = 0{\cdot}1$, $D_f = 0{\cdot}1$). (a) $\lambda_0 = 10$; (b) $\lambda_0 = 20$; (c) $\lambda_0 = 50$; (d) $\lambda_0 = 200$.

travelling velocity, and the transition from the bottom to the top is very sudden at a specific travelling velocity. Moreover, the increase of parameter μ, i.e., the density of cable, can greatly increase the above transition velocity.

Figure 7 shows the cable dynamics in the case of $\mu = 0{\cdot}1$. When the travelling velocity was low, e.g., $\lambda_0 = 10$, the cable had a few swings around the low-equilibrium position first and then returned to it as shown in Figure 7(a). With increase of travelling velocity, the stable equilibrium position of cable moved up and reached the plane of xoy as shown in Figure 7(b) when $\lambda_0 = 20$. To well understand this phenomenon, the global phase flow of equation (31) in this case is shown in Figure 8, where the equilibrium position at $\varphi_0 \approx 1{\cdot}571 \approx \pi/2$ is an asymptotically stable focus and the equilibrium position at $\varphi_0 \approx 4{\cdot}713 \approx 3\pi/2$ is an unstable saddle. If the travelling velocity is further increased, the cable would swing a few circles around the x-axis as shown in Figure 7(c) when $\lambda_0 = 100$ or even repeated many times as shown in Figure 7(d) when $\lambda_0 = 200$, and finally returned to the stable equilibrium position at the top. This phenomenon may cause troubles in marine engineering when an underwater cable is laid.

According to Figure 6, the cable density can greatly drop the equilibrium position and may reduce the possibility of large swing. Thus, the cable dynamics at $\mu = 0{\cdot}3$ was studied. Figure 9(a) shows the motion of mid-span section of cable when $\lambda_0 = 50$. In this case, the large density prevented the cable from getting up by nature, and made the cable swing with

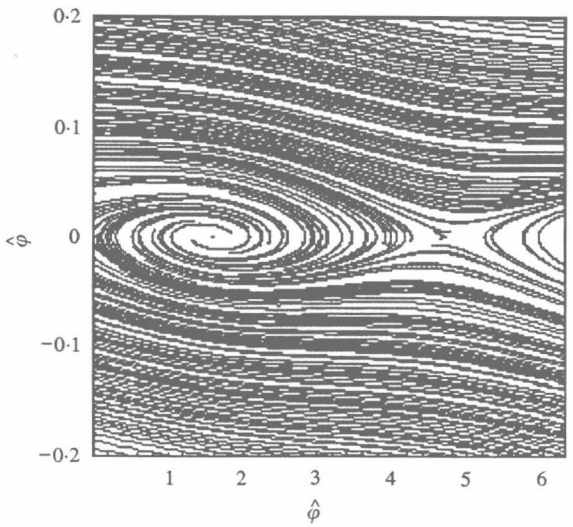

Figure 8. Global phase flow of equation (31). ($\mu = 0{\cdot}1$, $\lambda_0 = 20$, $d = 0{\cdot}1$, $c_f = 0{\cdot}5$, $v_f = 0{\cdot}1$, $D_f = 0{\cdot}1$).

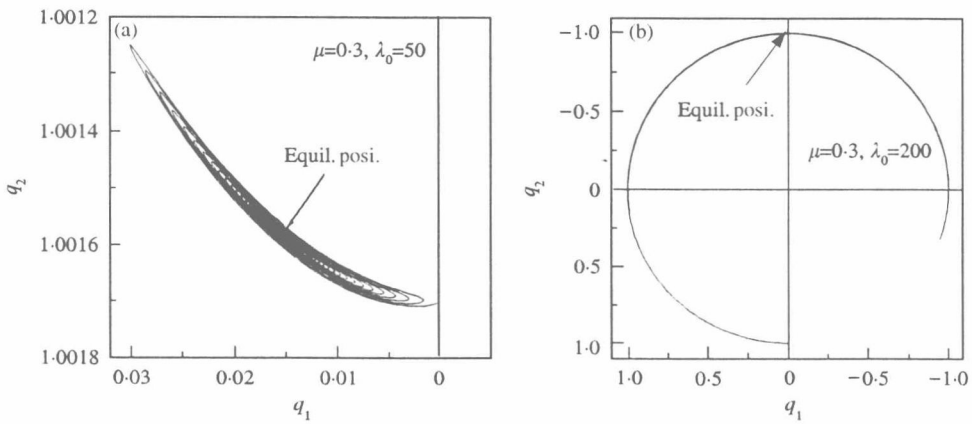

Figure 9. Motions of mid-span section of cable at different travelling velocities ($\mu = 0{\cdot}3$, $d = 0{\cdot}1$, $c_f = 0{\cdot}5$, $v_f = 0{\cdot}1$, $D_f = 0{\cdot}1$) (a) $\lambda_0 = 50$; (b) $\lambda_0 = 200$.

very small amplitude and return to the stable equilibrium position at the bottom. When $\lambda_0 = 200$, the stable equilibrium position of cable moved to the top as shown in Figure 9(b). Hence, the mid-span section of cable would undergo a couple of swings around the x-axis and settled down to the top equilibrium position at last.

7. CONCLUDING REMARKS

The motion of a suspended travelling cable subjected to transverse fluid flow can be approximately described by a two-dimensional autonomous system when the sag-to-span ratio is small and the Young's module of cable is large enough. In this case, the mid-span section of cable moves and vibrates like a spring pendulum. The cable has two equilibrium configurations. One is asymptotically stable and the other is unstable. With increase of